Available online at www.sciencedirect.com

ScienceDirect

Advances in Space Research 62 (2018) 3318–3334

ADVANCES IN SPACE RESEARCH (a COSPAR publication)

www.elsevier.com/locate/asr

Optical tracking and orbit determination performance of self-illuminated small spacecraft: LEDSAT (LED-based SATellite)

Fabio Santoni [a,*], Patrick Seitzer [b], Tommaso Cardona [c], Gianmarco Locatelli [d], Nicola Marmo [d], Silvia Masillo [d], Davide Morfei [d], Fabrizio Piergentili [c]

[a] Dipartimento di Ingegneria Astronautica, Elettrica ed Energetica (DIAEE), Sapienza – Universitá di Roma, Via Eudossiana 18, 00184 Rome, Italy
[b] Department of Astronomy of University of Michigan, 311 West Hall, 1085 South University Ave., Ann Arbor, MI 48109-1107, USA
[c] Department of Mechanical and Aerospace Engineering (DIMA), Sapienza – Universitá di Roma, Via Eudossiana 18, 00184 Rome, Italy
[d] Sapienza Space Systems and Space Surveillance Laboratory (S5Lab), Sapienza – Universitá di Roma, Via Eudossiana 18, 00184 Rome, Italy

Received 30 June 2017; received in revised form 8 August 2018; accepted 10 August 2018
Available online 22 August 2018

Abstract

LEDSAT is a 1U CubeSat developed by S5Lab team of Sapienza – University of Rome in collaboration with the Astronomy Department of University of Michigan. The main goal of the mission is to demonstrate that a LED-based active illumination system may be used to achieve orbit and attitude determination. LEDSAT will be placed into a Low Earth Orbit (LEO) and observed by a network of ground-based telescopes. A LED-based system may improve the accuracy in monitoring LEO spacecraft. A simple model is developed to estimate the features of an optical link between a ground station and a self-illumination system. The reliability of orbit determination and the precision of the orbit reconstruction is evaluated.

Keywords: CubeSat; Orbit determination; Attitude determination; Photometry; Space debris; Active illumination

1. Introduction

The large number of orbiting bodies in LEO is related to the advantages of space missions in close proximity to the Earth. The increasing interest in CubeSats and satellite constellations is contributing to the growth of the space population, which already counts more than 17,000 artificial objects with known orbits. The amount includes just a thousand of active spacecraft, considering sizes of more than 10 cm (Anz-Meador, 2017). Moreover, research on the instability of the space debris population indicates that, in the next 200 years, catastrophic and non-catastrophic collisions will lead to an increase of the LEO population, even without further launches (Liou and Johnson, 2016).

Continuous monitoring strategies of their orbits are required to perform conjunction analysis and operate collision avoidance manoeuvres among operative satellite and uncontrolled objects such as space debris (Inter-Agency Space Debris Coordination Committee, 2017).

Nowadays, orbit and attitude determination analysis are based on Passive Optical Tracking (Cardona et al., 2017), Satellite Laser Ranging (SLR) (Appleby et al., 2016; Kirchner et al., 2017), Radar, Radio telemetry, Global Navigation Satellite System (GNSS) (Nadarajah et al., 2012; Chang et al., 2016) and Doppler Orbitography and Radio-positioning Integrated by Satellite (DORIS)

* Corresponding author.
E-mail addresses: fabio.santoni@uniroma1.it (F. Santoni), pseitzer@umich.edu (P. Seitzer), tommaso.cardona@gmail.com (T. Cardona), gianmarco.locatelli@gmail.com (G. Locatelli), nicola.marmo.1@gmail.com (N. Marmo), silvia.masillo@gmail.com (S. Masillo), davide.morfei@gmail.com (D. Morfei), fabrizio.piergentili@uniroma1.it (F. Piergentili).

https://doi.org/10.1016/j.asr.2018.08.018
0273-1177/

(Brunet et al., 1995). Optical tracking includes all optical techniques that can provide information on the angular position of the satellite. Passive optical tracking of LEO objects is possible only when the object is in sunlight and the ground-based telescope is in darkness. This limits the tracking windows to a short time after sunset and before sunrise. Moreover, measurements are affected by weather dependence. Instead, radio tracking uses the radio frequency region of the electromagnetic spectrum, rather than the visible spectrum. Radars are used to track objects 10 cm and smaller in LEO (Walsh, 2013). Space debris laser ranging is a rather new field and measurements are possible only with cooperative targets that are equipped with retroreflectors (Hennegrave et al., 2013; Catalàn et al., 2015; Steindorfer et al., 2017).

In this framework, Sapienza Space System and Surveillance Laboratory (S5Lab) of Sapienza, University of Rome and Astronomy Department of University of Michigan (U-M) propose the innovative concept of optical tracking and the strategy is based on active illumination of the observed target. The proposed mission, called LEDSAT (LED-based SATellite), is based on a CubeSat equipped with coloured Light Emitting Diodes (LEDs) controlled to flash the light with specific patterns to be visible also when the satellites is in the Earth shadow (Seitzer et al., 2016, 2017). The 1U CubeSat will be deployed by the International Space Station (ISS) for a 1-year mission.

The idea comes from FITSAT-1 (Tanaka et al., 2015) mission, a Japanese 1U CubeSat, launched as a secondary payload on July 21st, 2012 from the ISS. It proved that a 1U CubeSat equipped with LEDs could be detected with ground-based small optical telescopes. LEDSAT mission focuses on further investigation on the nanosatellite tracking technique based on optical observations and aims to explore the potentialities of the flashing LED applications.

The S5Lab is highly involved into several projects related to space surveillance and space system design and development. Since 2011, Sapienza University of Rome, together with the Astronomy Department of U-M, are the main contributors of an international observing campaign of orbital debris for the Inter-Agency Space Debris Coordination Committee. Currently, the research teams are interested into the development of algorithms for orbit determination and new observing campaigns to improve the orbital accuracy and orbit trajectory prediction. Moreover, activities based on the analysis of light-curves have already lead to the development of a software for the reconstruction of attitude motion of orbiting bodies (Cardona et al., 2016a). The activities related to space system design made possible the development of the technological demonstrator URSA MAIOR (University of Rome la Sapienza Micro Attitude In Orbit testing) (Arena et al., 2015, 2016), a 3U CubeSat, launched on June 25th, 2017. URSA MAIOR may be considered a precursor for the LEDSAT project, since the satellite is equipped with two high power LEDs on two faces. Furthermore, in collaboration with the University of Nairobi, in Kenya, the projects of IKUNS (Italian-Kenyan University NanoSatellite) and 1KUNS (1st University NanoSatellite Precursor) have been conceived. Currently, they are under testing and assembling phase and the latter will be launched by December 2017 by the International Space Station.

Merging the experiences in space surveillance and nanosatellite development, LEDSAT mission aims to be a milestone for the improvement of the accuracy of orbit and attitude determination. Optical observations are often used for determining the orbit of uncooperative spacecraft and space debris and they provide the possibility to significantly improve the Two-Line Elements (TLE) orbital parameters estimation. However, a comparison between optical and other positioning data is not easily available for the uncooperative nature of the observed objects. LEDSAT mission provides the possibility to acquire optical data from an active and cooperative target, hence to verify and validate the optical stand-alone orbit determination techniques for space debris. The position data will be acquired both with an orbital Global Positioning System (GPS) receiver and retroreflectors, aimed at allowing laser ranging measurements. The attitude sensors data will be down linked and compared to the optical measurements. Moreover, the implementation of precise time synchronization system permits to collect high precision data even by using amateur optical telescope.

In this article, Section 2 concerns the LEDSAT mission and the ground segment of the project, while Section 3 focuses on the payload including image processing for orbit and attitude analysis. Section 4 is about the astrometry and orbit feasibility studies, while Section 5 outlines the applicability of LEDSAT mission, mainly concerning attitude determination and laser ranging allocation. Conclusions are presented in Section 6.

2. Mission concept

S5Lab research group is developing techniques to improve optical tracking and attitude determination algorithms. In this framework, the LEDSAT mission based on a 1U CubeSat equipped with LEDs and retroreflectors is proposed (Masillo et al., 2017).

To be visible for optical tracking, a satellite must be illuminated and observed against a dark-sky background, while the observer is in the darkness. The simplest source of illumination is the sunlight, when the spacecraft is outside the Earth shadow and its brightness is greater than the background sky. Hence, a LEO satellite is visible during twilight, while spacecraft in higher orbit can be observed beyond twilight and possibly all night.

Having an on-board LED-based payload gives LEDSAT active-illumination. For optical tracking of self-illuminated targets, the only condition is that the satellite must be above the horizon, the sky is dark, and with the LEDs switched on at the time of observation. Hence, the

time of detectability is extended to the whole period of eclipse (Seitzer et al., 2016).

Considering that star catalogues are provided with a precision of a few tenths of arc-seconds, by combining sidereal tracking and active illumination, the position of the satellite may be determined with very high angular accuracy. This is done by performing a satellite streak identification and centroid computation by processing images where the streak is superimposed on the background sky and considering satellite celestial coordinates, as will be discussed in Section 4. The validation of the optical standalone orbit determination technique will be done by cross-correlating the information provided by the on-board GPS receiver and laser ranging measurements, allowed by on-board retroreflectors, to the data obtained during the observation campaigns.

A further advantage is related to the implementation of the absolute timing of the LED flashes on the spacecraft itself in order to allow LEDSAT to autonomously execute the sequence of LED flashes. Hence, high timing precision on the ground-based system is no longer required and amateur optical ground stations can be involved in the network project.

A self-illumination system gives also the possibility to distinguish satellites in large cluster launches by making the spacecraft flash different patterns or having different colours of LEDs. In fact, if the objects appear very close to each other, optical observation of passive illuminated objects may lead to an incorrect target identification. Currently, the optical identification can be done only when the spacecraft reach certain angular distances between them. On-board LEDs may reduce time for data acquisition, resulting in an early recognition of the satellite.

Moreover, LEDSAT may be tested in several experimental modes, starting from LED light communication to attitude determination through simultaneous observations with different optical filters mounted on the ground telescopes.

2.1. Ground segment

The architecture of the optical Ground Station (GS) network, as shown in Fig. 1, for LEDSAT is composed by:

- MITO (Midlatitude ITalian Observatory), Sapienza University of Rome, Italy;
- EQUO-OG (Equatorial Italian Observatory On-Ground), Broglio Space Center, Malindi, Kenya;
- Zimmerwald Observatory, Bern, Switzerland (Schildknecht et al., 2003);
- Angel Hall Observatory, University of Michigan, Ann Arbor, State of Michigan, USA;
- MODEST (Michigan Orbital DEbris Survey Telescope), Cerro Tololo Inter-American Observatory (CTIO), Chile (Abercromby et al., 2011);
- SPADE (SPAce DEbris), Space Geodesy Center "Giuseppe Colombo", Matera, Italy.

The features of the optical network are described in Table 1.

Two GSs, located in Matera (Italy) and Bern (Switzerland) are included into the Laser Ranging GS Network. The main GS is located at S5Lab Urbe Airport GS, Sapienza University of Rome, Italy.

The pixel field of view (*PFV*) of every Charge-Coupled device (CCD) is evaluated by means of the equation:

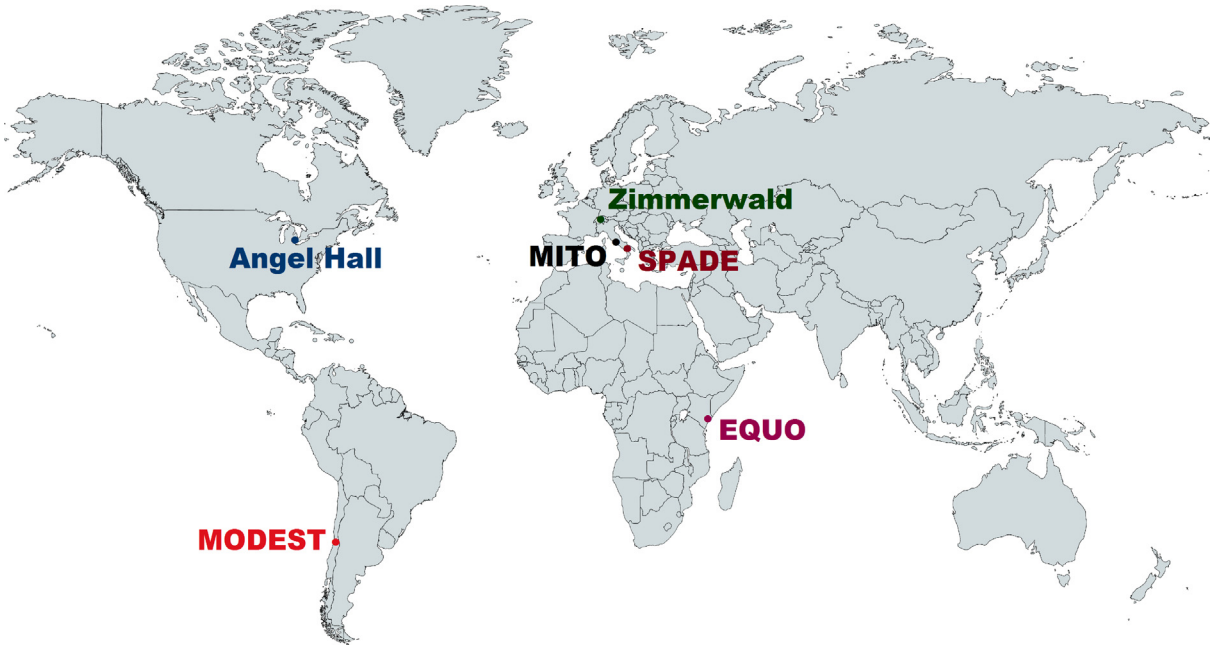

Fig. 1. Worldwide map of the optical GS.

Table 1
Telescopes and CCDs details of the GSs.

Observatory	Diameter of the entrance pupil (cm)	Focal ratio	CCD	Pixel size (μm)	CCD binning	Minimum elevation angle (deg)	Pixel field of view (arcseconds)
MITO, Rome (Italy)	25	f/3	E2V CCD42-40	13.5	2	20–35	7.44
EQUO, Malindi (Kenya)	20	f/4	FLI ML09000	12	4	30–50	12.39
Zimmerwald, Bern (Switzerland)	100	f/1.2	SI 1100	15	1	15–20	2.58
SPADE, Matera (Italy)	30	f/2.8	Proline 16803	9	4	25–40	8.85
Angell Hall, Ann Arbor (USA)	40	f/3	SBIG ST8	9	4	20–35	6.19
MODEST, CTIO (Chile)	60	f/3.5	E2V CCD231-84	15	2	22–35	2.90

$$PFV = 206.265 \cdot \frac{\mu_{ps} b}{f} \quad (1)$$

where μ_{ps} is the CCD pixel size in μm, f is the focal length of the primary in mm, b is a coefficient that takes into account the effect of the CCD binning on the pixel size, the constant value 206.265 is the arcseconds to radians conversion factor scaled by three orders of magnitude on account of pixel size expressed in μm and diameter in mm (Howell, 2006).

3. Photometry

3.1. Payload

The design of the payload depends on the detectability of the active illuminated system from the observatories of the project ground segment (Section 2.1), whose instrumentation capabilities are quite variable. Several analyses based on the signal and the apparent magnitude of LEDSAT at various altitudes confirm that the payload can be tracked by the whole network at a certain minimum elevation angle (MEA) and CCD binning. Photometry studies and constraints are extensively explained in Section 3.2, where the main features, the key advantages and limitations of the recommended selection of LEDs are clarified.

To fulfil mission objectives, LEDSAT is equipped with a total number of 140 high powered LEDs of three different colors. Considering a power budget suitable for CubeSat missions, the design of the LED-based payload is mostly driven by the efficiency of the LEDs, thus, the ratio between the radiated power, which is strictly linked to the luminous intensity, and the output power related to the voltage and the electric current. The number of components and the electronic circuit are a trade-off between the power budget and the efficiency of the devices. System configuration takes also into account mass and dimension constraints related to a 1U CubeSat standard structure. Moreover, the components are selected to withstand a proper range of operating temperature and variable voltage. The selection of the main wavelengths of the onboard illumination system is related to the highest Quantum Efficiency (Q_e) achievable by the CCDs of the scientific optical network. (Q_e), hence the greatest value of the ratio of incoming photons to those actually detected by the CCD, is associated to green and red for common image sensors. The design of the payload system has been aided by the development of a simulation tool able to calculate the LED flux as detected by each of the telescopes of the ground segment and by considering devices with different peak wavelengths and power levels. The following considerations are related to the final configuration:

- A stronger signal, and, consequently, detectable at a higher orbit altitude, may be obtained by considering wavelengths in the red spectrum;
- A good efficiency may be achieved by implementing blue LEDs, yet the atmospheric transmittance is significantly lower;
- A high luminous intensity, but with lower efficiency, can be achieved with green LEDs.

The final recommended configuration involves red, green and blue LEDs. It is important to underline that the classification and the analyses are based on the data sheets of the available commercial off-the-shelf (COTS) components and further tests in laboratory will be performed in order to evaluate the luminous intensity, viewing angle and efficiency. In particular, the simulations refer to the OSLON SIGNAL Series, manufactured by OSRAM Licht AG.

Moreover, the extreme challenging operating conditions must be taken into consideration. The space environment can lead to device failure for any space system. In particular, LED consists of a chip of semiconducting material doped with impurities to create p-n junction. The diode glows when a suitable voltage is applied to the leads and the electrons can recombine with the electron holes, falling into a lower energy level and releasing energy in the form of photons. The most common LED failure mode is the gradual lowering of light output and loss of efficiency. The testing campaign will obviously consider that semiconductor

electronics are inherently susceptible to radiation damage, by dedicating thorough tests on the LEDs.

To state with, LEDs are potentially sensitive to the total ionizing dose (TID) (Pritchard et al., 2003). Nevertheless, no sufficient information is found in the literature concerning the degradation of LEDs in space environment. Even though the accomplished mission of FITSAT-1 is a good starting point (Tanaka et al., 2015), LEDs have never been space qualified. Moreover, no space-qualified models are used as payload for LEDSAT. Complete functional and environmental qualification, performance and mission tests will be performed in order to understand if component degradation resulting from the TID or single event effects is sufficient to cause malfunction or catastrophic failure of LEDs.

3.2. Apparent magnitude and signal to noise ratio analysis

The feasibility and the accuracy of the orbit determination, as well as the number of possible observations, are related to the Signal to Noise Ratio (SNR) of LEDSAT on-board payload. For this reason, the S5Lab research group has developed a tool that evaluates the SNR and the bolometric apparent magnitude of the described system.

The bolometric apparent magnitude is independent from the characteristics of the optical instrument but gives useful information for the selection of the payload during the preliminary design phase. Precisely, it has been evaluated as:

$$m_{LEDs} = m_{Sun} - 2.5\,log\left(\frac{f_{LEDs}}{f_{Sun}}\right) \tag{2}$$

where m_{Sun} is the bolometric apparent magnitude of the Sun, f_{LEDs} is the irradiance of the LEDSAT payload and f_{Sun} is the solar constant, i.e. the mean solar irradiance at a distance of 1 AU. In particular, f_{LEDs} depends the total radiated power, P_{tot}, and the distance of the satellite from the observer, r, and it is calculated as:

$$f_{LEDs} = \frac{K P_{tot}}{4\pi r^2} \quad \left[\frac{W}{m^2}\right] \tag{3}$$

where K is a coefficient introduced to simulate the directivity of the LEDs. In particular, it is evaluated as the ratio between the solid angle of a sphere, representative of an isotropic radiation, and the solid angle of emissivity:

$$K = \frac{4\pi}{2\pi(1-\cos\theta)} \tag{4}$$

With θ equals to the apex angle of the LED emission. The hypothesis that K is homogeneous in the solid angle can be considered valid since the radiation characteristic of the selected LEDs is almost constant for about 150 degrees. In the presented analysis, COTS components produced by OSRAM have been considered, as previously mentioned in Section 3.1. The results related to the apparent magnitude are shown in Figs. 2 and 3, where the LED-based payload is fed with 30 W. The simulations are related to three different colors for an orbit height of 420 km (Fig. 2) and 650 km (Fig. 3). It is important to underline that the increasing trend of the curves depends on the distance, r, which is a function of the elevation angle.

As will be carefully explained in Section 4, the blinking time of the LEDSAT payload is scheduled to have both long and extremely short flashes, hence the streak will appear as composed by lines and dots. This is obtained by modulating the LED flashing time. It is important to remark that only the dots, which appear of the same relative dimension of stars in the CCD images, are used for the optical measurements. In the following, the extremely short flashing time is considered as the mean time of the passage of the target over a single pixel (t^*). This assumption allows to treat the dots as Point Spread Functions (PSFs) for the evaluation of the SNR. The resulting SNR strongly depends on the GSs, due to the characteristics of the telescopes and the CCD sensors. According to the unofficially named CCD Equation (Howell, 2006):

$$SNR = \frac{\alpha N^*}{\sqrt{N^* + n_{pix}\left(N_{sb} + N_{db} + N_R^2\right)}} \tag{5}$$

where the signal term, N^*, is the total number of photons from the source collected by the CCD during the previously mentioned time, t^*, and α is the fraction of N^* gathered in the CCD area utilized for the SNR calculation of the PSF, namely aperture. The coefficient α is a function of the ratio between the selected aperture radius and the Full Width at Half Maximum (FWHM) of the PSF (Howell, 2006). The noise term behaves under the auspices of Poisson statistic. It is the square roots of N^*, plus the number of pixels inside the aperture, n_{pix}, times the contribution from the total number of photons per pixel resulting from the sky background, N_{db}, the total number of dark current electron per pixel, N_{db}, and the total number of electron per pixel due to the read noise, N_R^2.

While N^* is related to the time of passage over one pixel, the sky shot noise and the dark current are linked to the exposure time. A linear trend of N_{sb} and N_{db} with the exposure time is considered. The values of N_{db} and N_R^2 have been acquired within the CCD datasheet, while N_{sb} has been obtained processing the available images gathered with the selected GS.

It is important to remark that n_{pix}, right hand side of Eq. (5), has been calculated by considering the apparent pixel size, which is related to the CCD pixel size and the CCD binning. Precisely, the binning considers how the pixels are summed, in vertical or horizontal direction, in the output register (Howell, 2006).

By relating the noises terms, N_{sb} and N_{db} to the binning:

$$N_{db} = B N_d t_{exp} \quad [e^-] \tag{6}$$

$$N_{sb} = B N_s t_{exp} \quad [e^-] \tag{7}$$

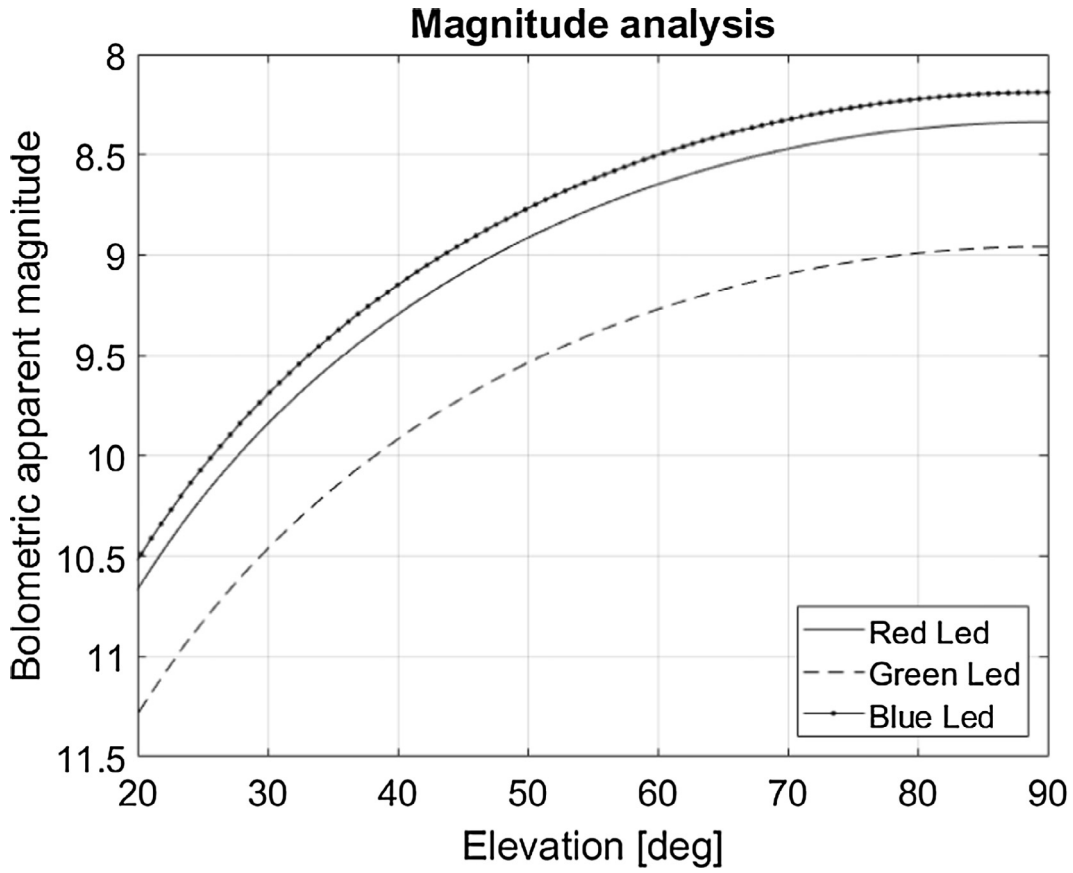

Fig. 2. Apparent magnitude of LEDSAT at an orbit height of 420 km.

where B is the number of CCD pixels contained in an apparent pixel, t_{exp} is the exposure time, N_s and N_d are respectively the signal coming from the sky background and the dark current, both expressed in electrons per pixel per second.

Considering that the presented SNR analysis is valid only if the source can be treated as a PSF, only the dots of the luminous pattern can be considered. If the blinking time is greater than t^*, that time has to be used instead of t^*. Moreover, all the pixels swept by the target streak have to be regarded in the calculation.

By assuming that flux irradiated by the LEDs is monochromatic, the CCD response to the incoming photons is described by a value representative of the Q_e and function of the wavelength. In fact, Q_e expresses the ability of the detector to turn incoming photons into useful output. In addition, this assumption allows to convert the LED based-payload irradiance into photons flux, by considering only the peak wavelength of the LEDs.

The total number of photons collected from the object of interest, N^*, has been obtained as:

$$N^* = f_{LEDs} t^* Q_e(\lambda) \frac{\lambda}{hc} A_T \tau_A \tau_T (1 - O_s) \ [e^-] \tag{8}$$

where the LED flux, f_{LEDs}, is previously calculated in Eq. (3), $Q_e(\lambda)$ is the CCD quantum efficiency at the peak wavelength, λ, h is the Planck constant, c is the light velocity, A_T is the telescope mirror area, τ_A is the atmospheric transmittance, τ_T is the telescope transmittance and O_s is the obstruction due to the secondary mirror of the telescope. The latter is obtained as the ratio between the area of the secondary and primary mirrors, and it is equal to zero for refractive telescopes. In a preliminary analysis, by taking into account that for colored LEDs the emission band is about 50 nm thick, the atmospheric response can be considered almost constant in the band (Nitschelm, 1988).

Moreover, the dependence of τ_A on the elevation angle is neglected, hence significant discrepancies are expected at very low elevation. Nevertheless, if a minimum elevation angle of about 30° is used for the optical observations, the model can be considered acceptable.

Figs. 4 and 5 show the SNR in function of the elevation angle. The analysis is related to LEDSAT with the previously mentioned configuration, at an orbit height of 420 km, as detected by MITO ground telescope. In particular, Figs. 4 and 5 consider the 100% and the 50% of LEDs switched on, respectively. The second condition could be representative of a particular operational mode that requires the simultaneous lighting of two faces, or a failure of the half of the devices.

Moreover, an average value of 5 arcseconds (FWHM) for the seeing has been considered. The latter refers to the blurring and twinkling of astronomical objects.

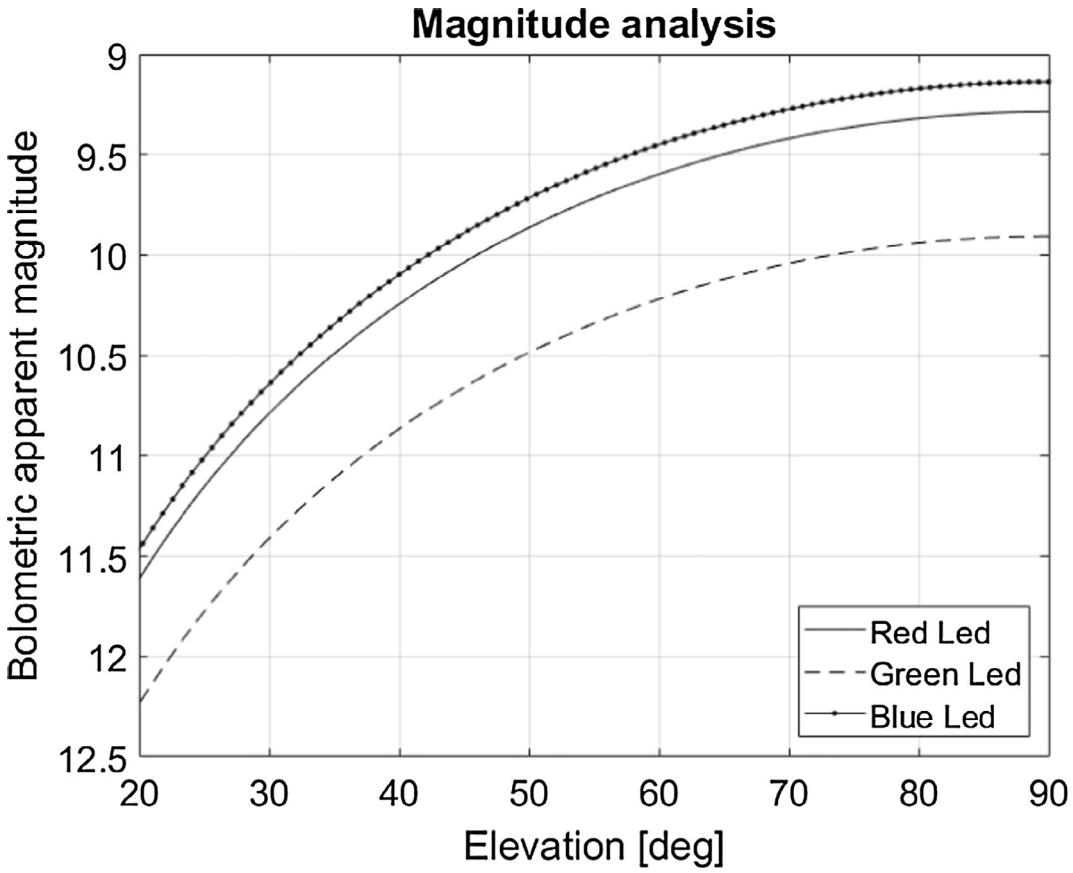

Fig. 3. Apparent magnitude of LEDSAT at an orbit height of 650 km.

Finally, Fig. 6 shows SNR trend if the 50% of LEDs is switched on and the CCD is working with a 2×2 binning instead of 1×1 binning. The kind of binning has been chosen as the most suitable for an acceptable SNR and a good resolution.

As shown, red LEDs exhibit the best performances due to the best response of the CCD to the red spectrum. On the other hand, the blue LEDs have a greater efficiency, hence, for the same input power, the blue devices have a greater output flux. Moreover, even considering the lower atmospheric transmittance and the inferior CCD response, their performances are acceptable according to the SNR trend.

A minimum acceptable value of SNR of 10 allows a good detection. Recalling the simulation shown in Fig. 4, every coloured LED configuration is visible with a MEA of 40°, 60° and approximately 70° for red, blue and green LEDs, respectively. By analyzing Fig. 5, where the half of the LEDs are switched on, it is evident that there is no visibility for the blue and green LEDs.

Nevertheless, by increasing the CCD binning, t^* becomes greater, hence the collected signal, N^*, is higher. Furthermore, the readout noise is reduced and even if the sky shot noise slightly increases, the resulting SNR is more acceptable. Thus, as shown in Fig. 6, also the green and blue LEDs are detectable. However, the higher the binning, the lower the optical resolution, and, therefore, the accuracy of the measurements.

Table 1, in Section 2.1, shows the MEA and the CCD binning for all the GS of the network. MEA is expressed as a range due to its dependency on the LED colour.

In June 2017, 3U CubeSat URSA MAIOR, developed by S5Lab research team, has been launched (Arena et al., 2015, 2016). The CubeSat is equipped with four high power LEDs, similar to the ones mounted on LEDSAT, as shown in Fig. 7. Therefore, it can be considered a precursor for LEDSAT and test will be performed to identify valuable solution for flashing strategy that will be implemented in the mission. The analysis performed on the apparent magnitude of the 3U CubeSat are shown in Fig. 8.

4. Astrometry for precise position

Images made by a sensor connected with a telescope are used for orbit determination. In case of objects without active illumination, the observed quantity is the solar flux reflected by the surface. The exposure time is calculated in order to detect also the background stars whose position is available through star catalogues. Star recognition algorithm based on oriented triangles (Rousseau et al., 2005) are used to assign the coordinates of particular points of the streak which are usually the midpoint and the

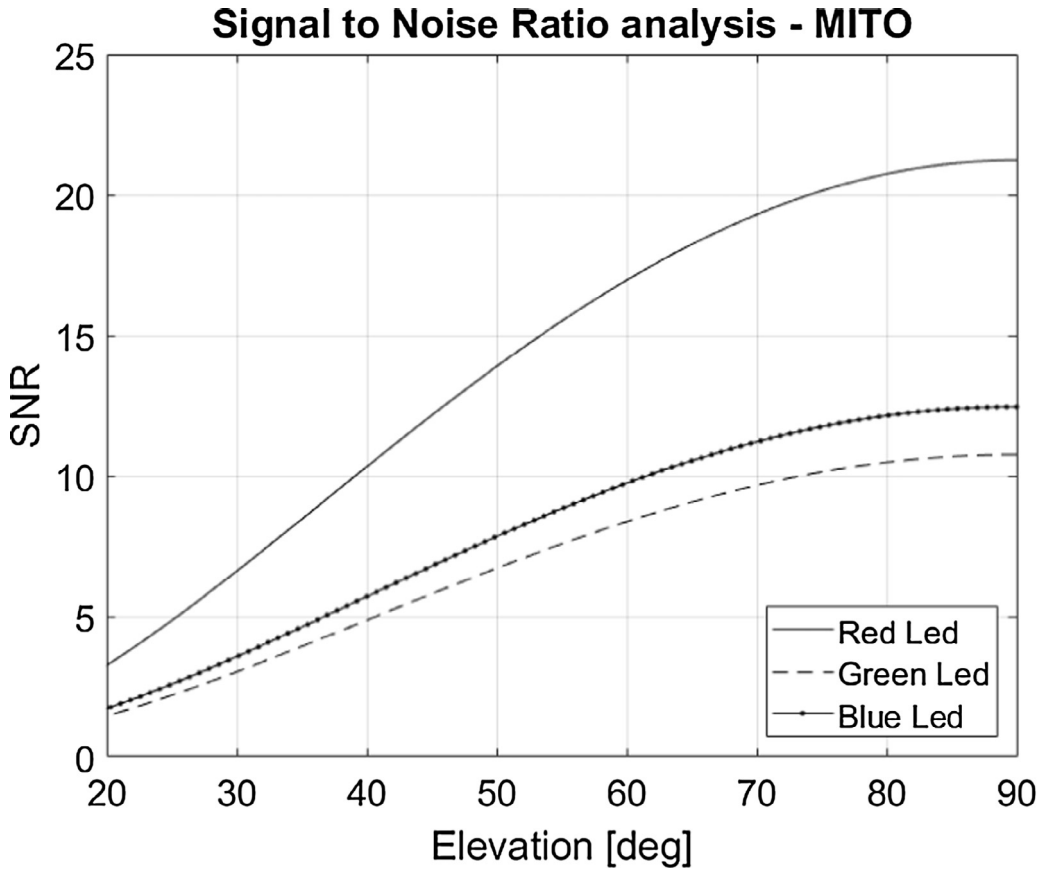

Fig. 4. SNR analysis for MITO, Rome – binning 1 × 1 – 100% LEDs switched on.

endpoints. The first one is positioned on the geometric centre of the trail and the assigned epochs generally correspond to the start of the observing time plus half of the exposure time set. Nevertheless, LEO objects might have a non-uniform velocity along the track and the previous consideration may not be valid. For this reason, it is possible to assign a time-tag only to the endpoints. These time tags are respectively the initial and final epoch of exposure. An example of the optical signature of a LEO object is shown in Fig. 9.

The magnitude of the streak is not constant, this variation might be connected to changes of the solar phase angle and possible tumbling motion or attitude variation of the orbiting object. This means that the magnitude of the trail might be less than the background sky. Therefore, the streak appears as a series of disconnected flashes. When one of the magnitude minimum occurs at the extremes of the trail, the determination of the endpoints is uncertain (Somers, 2011). Different methodologies are being studied to solve this problem (Cardona et al., 2016a,b). LEDSAT innovation consists in using an active illumination system and an external high-stable oscillator to trigger the LEDs according to a scheduled pattern. For orbit determination, the latter will be a series of dots and lines. The points will have the same relative size of the stars in the background in order to assign their coordinates with high precision. Different simulations have been made in order to obtain the flashing time that meets this condition; an approximate value is about 10 ms. The alternation of lines and points gives the observer precise information about the time in which the signals are generated from the payload. This system permits to associate the generation of each point or line to a precise instant. Two simulations of different luminous patterns are shown in Fig. 10.

The described simulations performed to identify, on the collected image, the satellite of the same relative dimension of a star, show that the obtainable accuracy is also closely linked to the accuracy of the time coordinates: therefore, the higher the time accuracy of the ground station, the higher the precision of the acquired data.

Precise time synchronization between the satellite and the GSs is necessary to correctly flash the LED pattern and allow LEDSAT to be used as calibration target. This requirement may not be satisfied by using the On-Board Computer (OBC) oscillator, as the time would drift beyond the acceptable threshold, if the on-board GPS is disconnected. For this purpose, LEDSAT is equipped with a high precision time keeping device. By using both the GPS and an external Temperature Compensated Crystal Oscillator (TCXO) or an Oven-Controlled Crystal Oscillator (OCXO) to propagate the GPS time, the drift will be kept low. Precisely, these devices have an ageing coefficient of few tens of parts-per-billion (ppb) and, compared to the GPS-UTC time, the time drift will be of 1/60 s in an

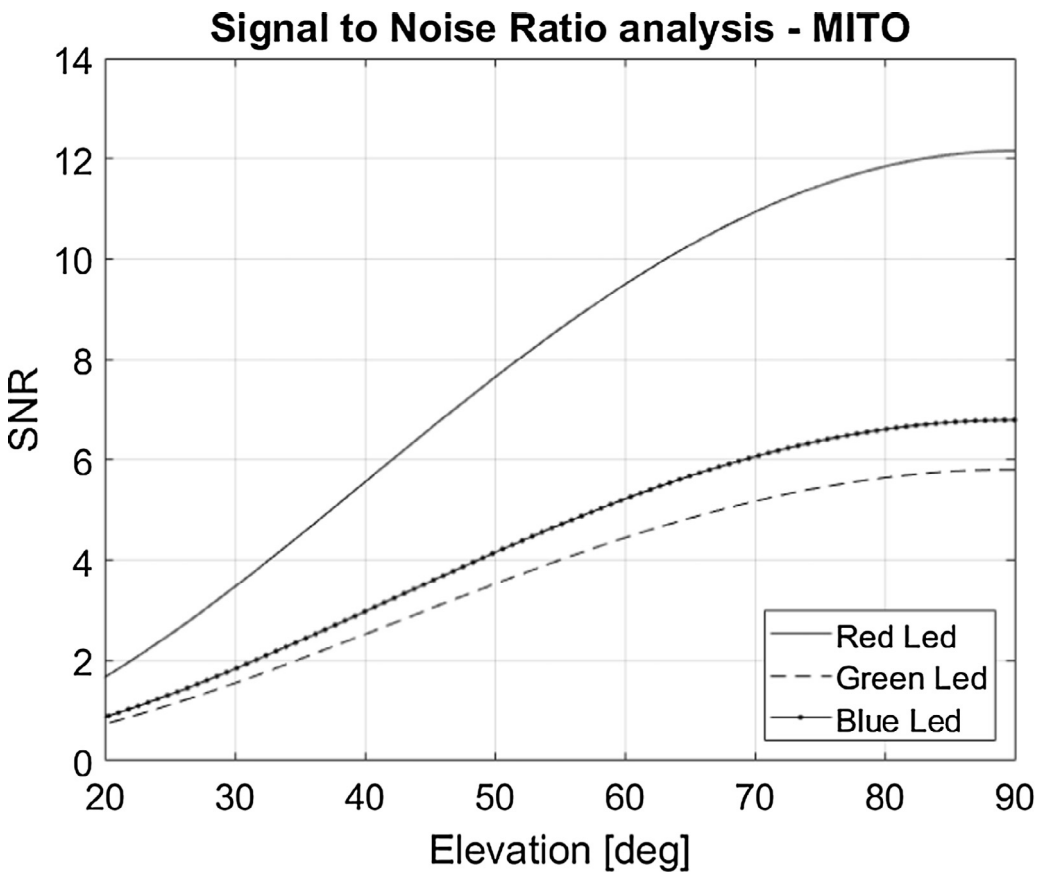

Fig. 5. SNR analysis for MITO, Rome – binning 1 × 1 – 50% LEDs switched on.

interval between 10 and 40 days for the TCXO and OCXO, respectively. Moreover, the drift will be monitored by downlinking the data, taking into account TX/RX delays, and by planning synchronizations of the GPS time with the information experimentally obtained by the selected external oscillator.

By employing both the internal and the external clock, matched with the illumination system, the time at which the flash occurs will be known with high precision. Hence, tracking data may be obtained without the need of high accuracy time-keeping ground stations.

4.1. Feasibility study for orbit determination

The feasibility assessment of the orbit determination has been carried out through the simulation of the expected measurements and the implementation of a batch filter to process them. The results of the simulations of different scenarios have been considered in order to evaluate the system performance.

The considered observables are the angular measurements of the satellite. Measures have been taken every 60 s during the satellite-ground stations visibility windows over a period of 12 h or 24 h depending on the combination of observatories which are used to track the satellite.

An orbit propagator which takes into account the effect of both J2 perturbation and drag has been used to obtain the satellite position along the trajectory. The observables have been obtained by adding a White Gaussian Noise proportional to the real accuracy of each observatory to the exact angular position.

A wrong guess set of ephemerides has been used to initialize the batch filter. This initial state has been obtained from the exact state by considering an error on the norm of the position of 10 km and an error on the norm of the velocity of 100 m/s.

The norm of the difference between observables and angular measurements obtained from the propagated guess initial state gives the following cost function J:

$$J = \sum_i (RA_i - \tilde{RA}_i)^2 \cos^2(DEC_i) + (DEC_i - \tilde{DEC}_i)^2 \qquad (9)$$

where RA_i and $\tilde{RA}_i$ are the propagated and observed right ascension angles, and DEC_i and $\tilde{DEC}_i$ are the propagated and observed declination angles.

Through an iterative procedure, the filter finds the initial state vector which minimizes the cost function and, by knowing the real initial state, the difference between them can be evaluated; this difference represents the error on the initial state reconstruction.

In order to emulate different conditions of tracking, several combinations of observing ground stations and periods of data collection have been considered:

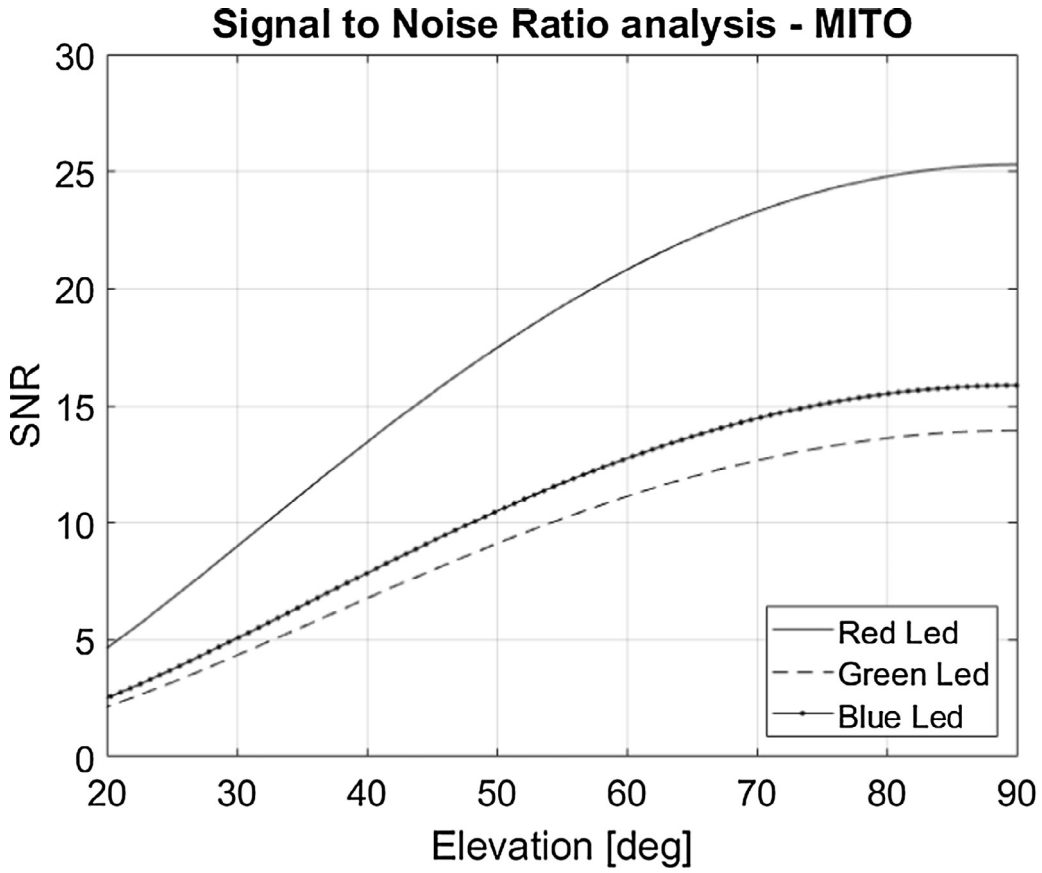

Fig. 6. SNR analysis for MITO, Rome – binning 2 × 2 – 50% LEDs switched on.

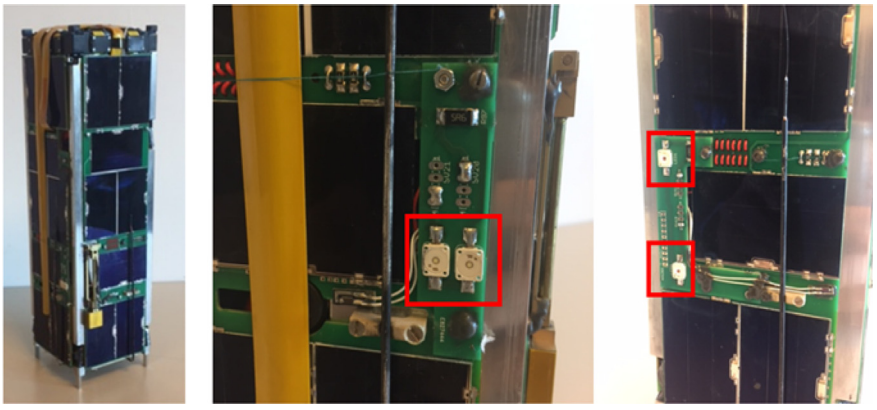

Fig. 7. URSA MAIOR and on-board LEDs.

- EQUO-OG and MITO for 24 h;
- Angel Hall Observatory and SPADE for 12 h;
- MODEST and MITO for 24 h;
- MITO for 24 h;
- Zimmerwald Observatory for 12 h;
- All the observatories for 12 h.

For each scenario, 60 Monte Carlo simulations have been carried out to evaluate the performance of the orbit determination; all the simulations use the same initial state to start the iterative process. In all the 6 scenarios, orbit determination has been achieved with good precision.

The graphic representation of the reconstructed initial positions obtained by orbit determination for each case is shown in Figs. 11–16 using a Local-Vertical-Local-Horizontal (LVLH) orbital reference frame centered on the exact initial position. The $\hat{r}$ axis has the same orientation as the position vector of the satellite with respect to an inertial reference frame originated in the centre of the Earth, the $\hat{\theta}$ axis has the same orientation as the velocity vector of

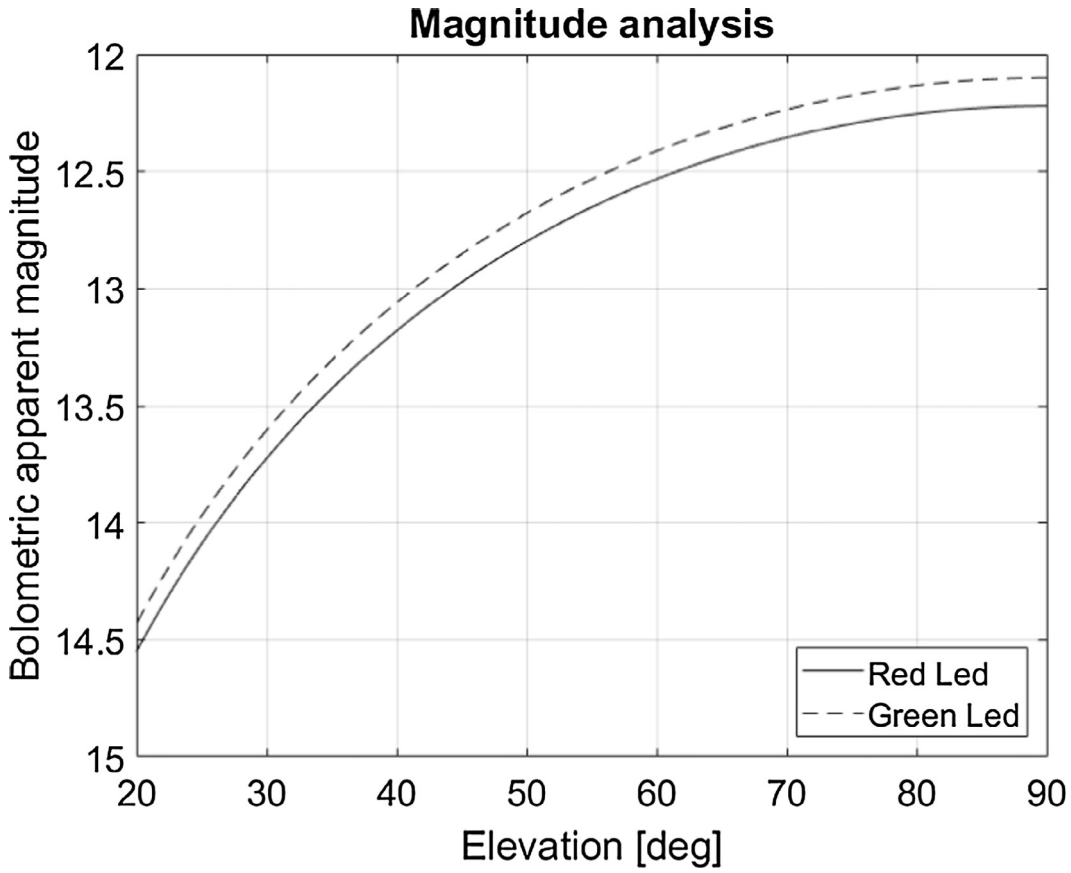

Fig. 8. Apparent magnitude analysis for URSA MAIOR at the altitude of 510 km.

Fig. 9. Optical signature of a LEO object.

the satellite, the $\hat{h}$ axis completes a right-handed reference frame.

The initial state reconstruction provides accurate results. The main component of the position error is in the $r\theta$ plane while the one along the h direction is very small. The validity of the orbit determination is also confirmed by the statistical analysis which has been carried out on the results. The numerical outcomes of this analysis are shown in Tables 2 and 3.

All the three components of the velocity error are very small in all the cases and it proves that the initial velocity has been reconstructed with extremely high accuracy.

Another important outcome is that using measurements obtained from only one of the ground stations leads to less

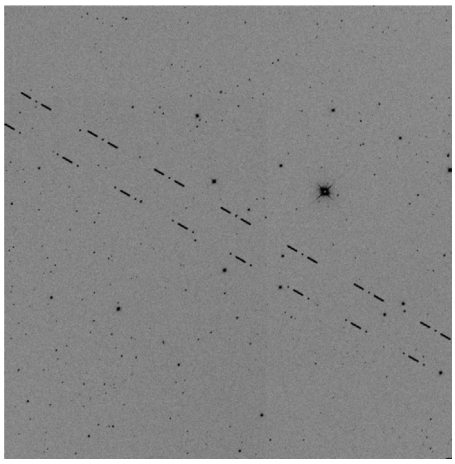

Fig. 10. Simulation of two satellites flashing with different luminous patterns. The simulated signals are superimposed on a real image collected by Curtis-Schmidt telescope in Chile.

precise results than those which are obtained by including also data from other observatories.

The higher precision of the initial state reconstruction achieved by tracking the satellite using MITO and EQUO-OG or MITO and MODEST instead of using only MITO confirms the previous consideration.

5. Attitude determination

As previously described in Section 2, active illumination on the CubeSats increases the number of passes in which they can be tracked. By removing the dependence of brightness on topocentric solar phase angle, there is no more a limited number of passes in evening or morning when the telescope is in darkness and the satellite is in sunlight. Simulations show (Seitzer et al., 2016) that for an orbit like the one of ISS, it is possible to increase the number of daily

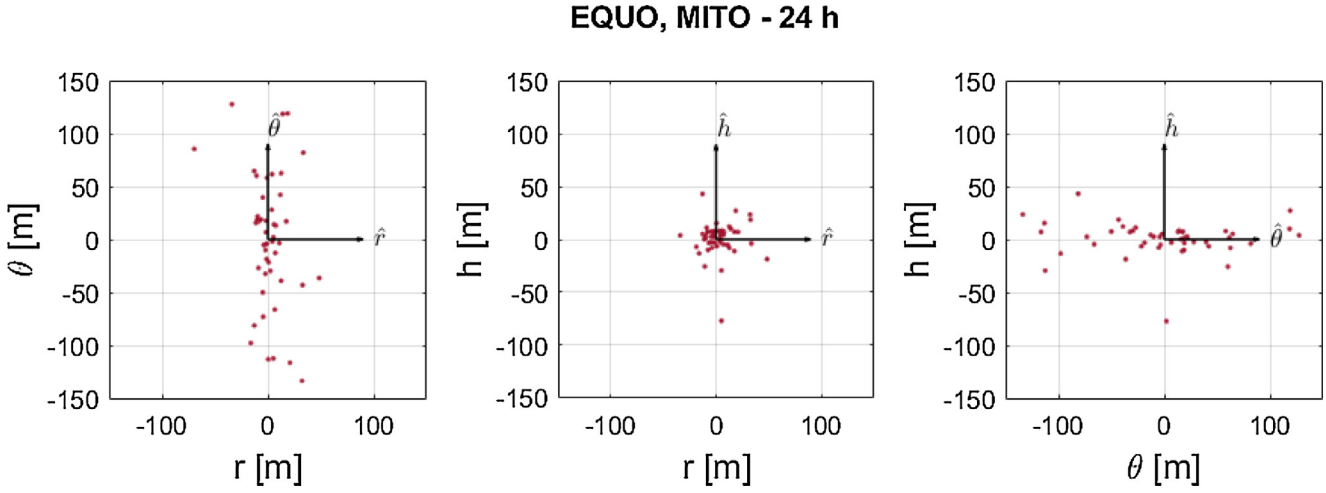

Fig. 11. Orbit determination results obtained by observations made by MITO and EQUO over a period of 24 h.

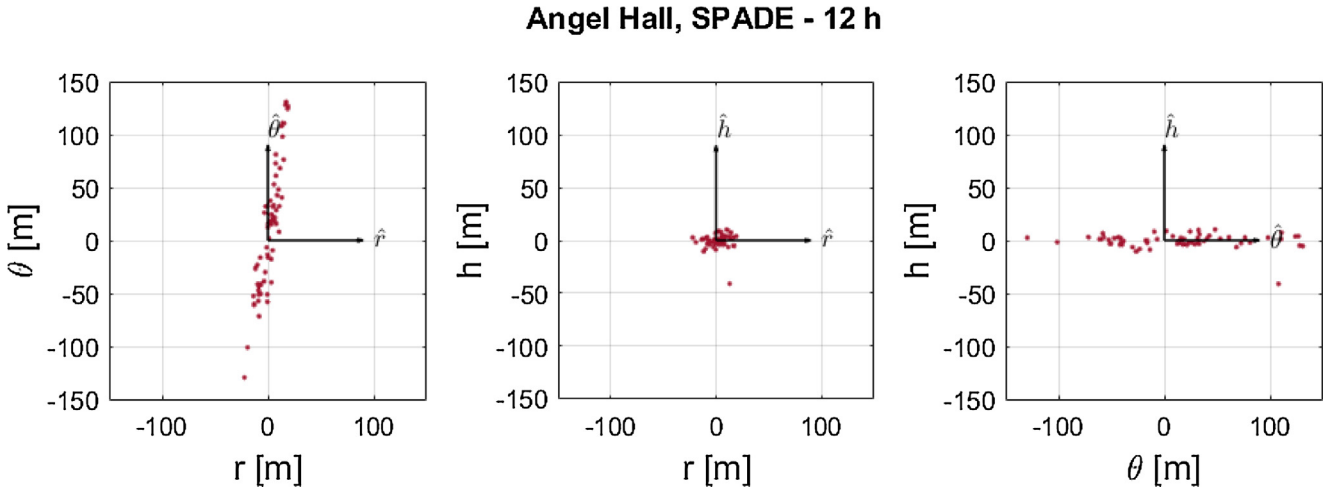

Fig. 12. Orbit determination results obtained by observations made by Angel Hall Observatory and SPADE over a period of 12 h.

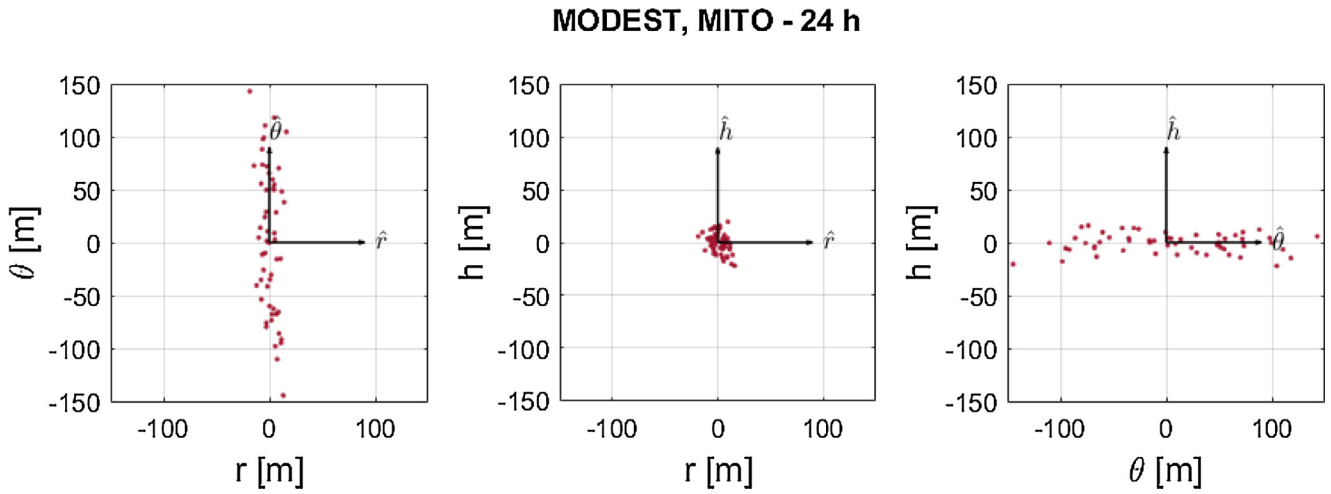

Fig. 13. Orbit determination results obtained by observations made by MODEST and MITO over a period of 24 h.

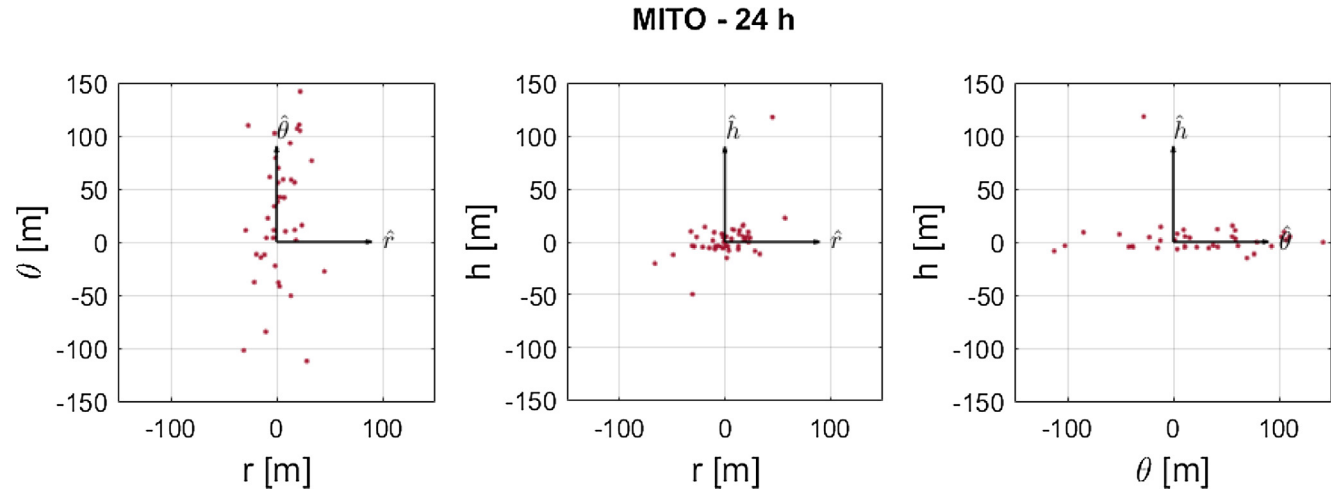

Fig. 14. Orbit determination results obtained by observations made by MITO over a period of 24 h.

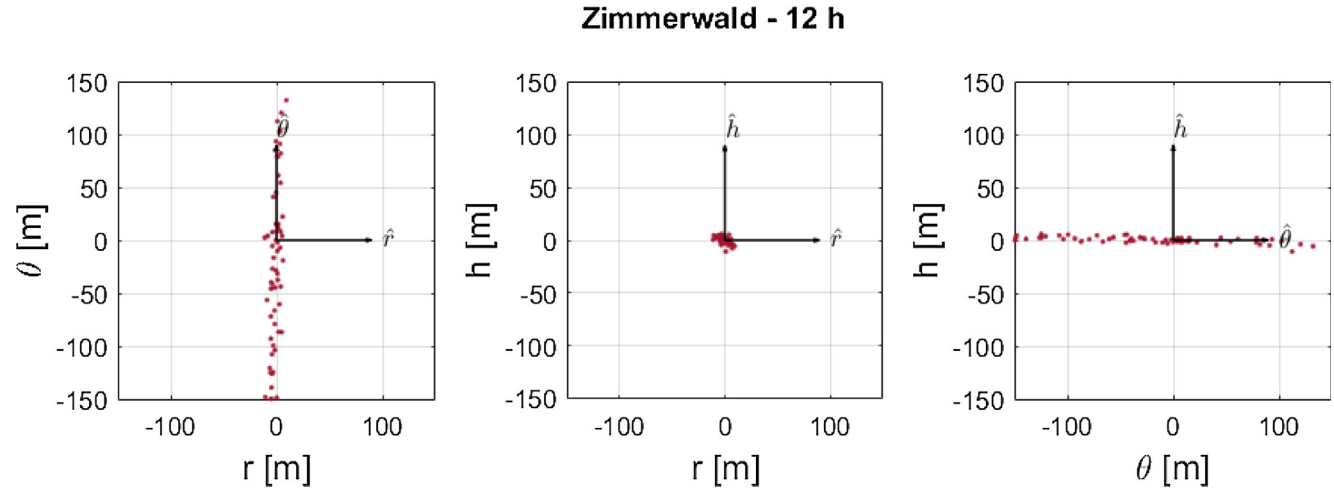

Fig. 15. Orbit determination results obtained by observations made by Zimmerwald Observatory over a period of 12 h.

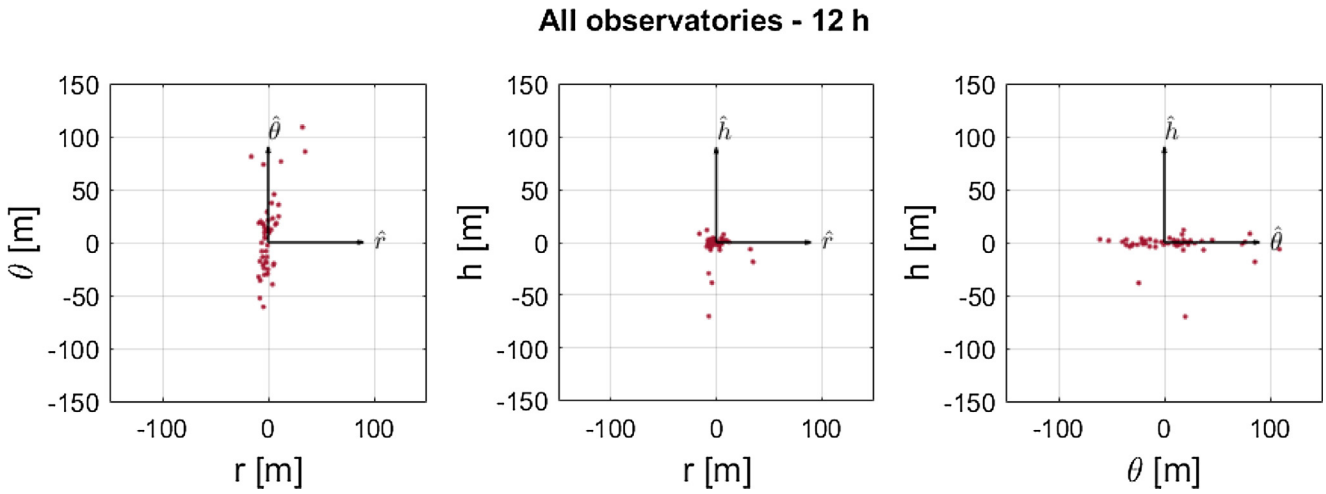

Fig. 16. Orbit determination results obtained by observations made by all the ground stations over a period of 12 h.

Table 2
Statistical analysis of the position error.

		EQUO, MITO 24 h	Angel Hall, SPADE 12 h	MODEST, MITO 24 h	MITO 24 h	Zimmerwald 12 h	All GSs 12 h
Position error r direction (m)	Mean	1,3749	1,4738	0,7049	0,9255	−0,6958	−0,1540
	Std. dev.	17,8767	9,6990	7,5577	22,4110	4,4351	8,9562
Position error θ direction (m)	Mean	0,4036	11,1415	2,1757	36,4422	−12,7767	9,4035
	Std. dev.	75,2473	58,9451	74,6208	97,0076	89,8531	42,3891
Position error h direction (m)	Mean	−3,1792	−0,5737	−0,6079	1,8931	0,0133	−3,1665
	Std. dev.	29,8552	6,8192	9,4612	20,1189	3,2373	12,5155

Table 3
Statistical analysis of the velocity error.

		EQUO, MITO 24 h	Angel Hall, SPADE 12 h	MODEST, MITO 24 h	MITO 24 h	Zimmerwald 12 h	All GSs 12 h
Velocity error r direction (m/s)	Mean	0,0001	−0,0099	−0,0026	−0,0310	0,0105	−0,0067
	Std. dev.	0,0666	0,0501	0,0764	0,0818	0,0763	0,0346
Velocity error θ direction (m/s)	Mean	−0,0016	0,0016	−0,0008	−0,0010	0,0009	0,0001
	Std. dev.	0,0204	0,0109	0,0090	0,0255	0,0049	0,0101
Velocity error h direction (m/s)	Mean	0,0026	−0,0008	−0,0012	0,0073	0,0011	0,0091
	Std. dev.	0,0248	0,0154	0,0155	0,0267	0,0166	0,0387

passes over a midlatitude ground station by a factor of three to an average of almost three passes per night.

The increase of total number of daily passes provides not only an improvement in orbit determination capabilities, but also a way to reconstruct the attitude of the satellite by using its light-curves. In fact, the idea of the LEDSAT project is then to collect light-curves emitted in different LED colours from optical ground-based observatories and to process them for both orbit determination and attitude reconstruction.

Generally, orbiting object do not have a constant brightness. They reflect the sunlight as flashes at typically regular times that are caused by their tumbling motion. Brightness changes over time-scales of a second or less can be investigated using long exposures by trailing the target across the field of view while the telescope is sidereally tracking. The result is an image where the target appears as a streak while the background stars appear as dots. The counts distribution in the along-track dimension of the streak is used to detect the primary frequencies of the satellites (Cardona et al., 2016a).

By flashing the LEDs with specific patterns in different colours data useful for attitude reconstruction can be collected. S5Lab research team has developed an automatic pipeline (Cardona et al., 2017) to process satellites light-curves for main frequencies extraction. The success in the determination of the main frequencies depends mostly on the accuracy of the measurements of the flash peaks. The background sky median level is evaluated according to 2-dimensional spread function (PSF) of the streak. The streak ends are therefore evaluated as the points where the total count in the along-track dimension is comparable

with the median value of the sky level previously evaluated (Somers, 2011). Their accurate determination is crucial for a precise attitude reconstruction. Due to the flashing pattern of the LEDs, when a flash occurs near the beginning or end of the time exposure, the location of the end is obscured, and a solving strategy must be considered. For an accurate and precise timing, LEDSAT is designed to have an on-board clock to assign a time tag to each generated LED pulse of the pattern. This allows to solve the streak end uncertainty and even simple ground-based telescopes would take sidereally tracked images without the need of a millisecond timing accuracy and precision at the telescope (Seitzer et al., 2016).

A method based on a 3-D virtual reality model of the target itself has been tested to reconstruct the attitude of the satellites (Piergentili et al., 2017). This tool uses simulated light-curves obtained for the virtual model and real measurements to determine the attitude.

As previously said, light-curves are strictly connected with the materials and the shape of the external surface of the satellites. Therefore, it is crucial to reconstruct the virtual model of the satellite with an accuracy as high as possible. All the details of the spacecraft will be implemented in the model including external surface material properties, mass and momentum of inertia, LED central wavelength, radiant power emitted by the LEDs, the total number of them and their disposition in the satellite reference system. All these parameters will be characterized with laboratory measurements during the test phase.

The core of the tool is the processing phase based on genetic algorithms. The virtualized model of the satellites is used to be processed by considering Euler equation of rigid body. The real measured light-curves are used to be compared to the simulated ones as input into a cost function for the multi-objective optimization process. By minimizing the root mean square of the residuals, the real attitude of the satellites that produces the measured light curves can be extracted (Piergentili et al., 2017).

The method is then used to identify a set of rotation parameters of the CubeSat compatible with the measured light-curves. Moreover, the results will be compared with the attitude obtained from the Attitude Determination and Control System (ADCS) and will be used to validate the developed tool.

5.1. Data fusion: LED-based payload and SLR

Telemetry from ADCS and LEDs light-curve measurements can provide valuable data for both orbit and attitude determination. These two different methodologies are both based on active payload. In case of a failure on one of these subsystems no information might be provided. For safety reason of the LEDSAT mission, it is crucial to include also passive systems for redundancy such as cube-corner reflector for laser ranging measurements. SLR is the most accurate technique currently available to determine the geocentric position of an Earth satellite and to perform range measurements to cooperative satellite, equipped with retro laser reflectors, that allow attitude and spin period determination (Kucharski et al., 2014). In fact, the application of retroreflectors, even in small satellites such as CubeSat, are multiple: independent precise orbit determination (POD) also after end-of-life, attitude determination using multiple laser retroreflectors and verification of satellite attitude sensors via laser retroreflectors (Kirchner et al., 2013).

For these reasons, LEDSAT is designed to be equipped with four retroreflectors (two on the top panel and two on the bottom ones) that can ensure the reflection of the 98% of the incident laser beam between 500 nm and 800 nm. Kirchner et al. (2013) demonstrated that around 50 mm distance between two retroreflectors should permit to ensure information about the attitude with an accuracy of around 1 degree independent of operational status of the satellite.

Besides this application, it has been demonstrated (Cordelli et al., 2016) that the accuracy of OD can be improved by merging and combining different kind of observables, i.e. laser ranging measurements and optical data as input for both radial and angular data. The development of these techniques is crucial for the precise knowledge of the positions of the orbiting objects. The process accuracy relies also on the type of observables used, their accuracy and the length of the observed pass. Moreover, by adding LEDs for optical measurements, the number and the duration of satellites passes are enlarged.

6. Conclusions

The S5Lab research team and the Astronomy Department of U-M have proposed the project of LEDSAT, a 1U CubeSat equipped with coloured LEDs and retroreflectors, used as technological demonstrator for optical observations in LEO.

The main goals of the mission are related to the improvement of the accuracy of orbit and attitude determination. The mission aims to explore the potentialities of a self-illumination system, ranging from the increase of number and duration of passes in which the satellite is visible, to the possibility of the immediate identification of the spacecraft in cluster launches. Further applications are related to LED light communication and the prospects of using a satellite as calibration target for optical ground stations, by placing the absolute timing on the spacecraft itself.

MITO, the optical ground station at Sapienza University of Rome, is included in a network of six observatories spread worldwide. The main requirement of the LED-based payload is the detectability from the whole network, confirmed by photometric studies. To fulfil the mission objectives a configuration based on three colours of LEDs and retroreflectors have been recommended and considerations about the possible failures of electronic devices in the space environment have been carried out. The software

developed for the evaluation of the detectability of the LED-based Satellite by the optical network has been carefully described. The tool allows also to get useful information for observations, such as the kind of CCD binning and the MEA, and to define the final configuration of the LED-based payload. Moreover, LEDSAT magnitude and the SNR for MITO telescope have been presented. Further analyses have been carried out on URSA MAIOR, an already launched 3U CubeSat equipped with LEDs similar to those mounted on LEDSAT.

The orbit of LEO objects can be determined through the optical signature recorded by telescope camera sensors. Nevertheless, there are uncertainties related to the centroid and the magnitude of the streak. An on-board active illumination system and a precise oscillator, used to trigger the LEDs in a defined flashing time, may allow even amateur telescope to reach high-accurate measurements.

Making use of the results obtained by the SNR analysis, a feasibility study for the orbit determination has been carried out by simulating angular measurements of the satellite and processing them with a batch filter. The results show that orbital determination can be achieved with high accuracy even considering different scenarios in terms of operating ground stations and observation times.

In the end, the application of light-curves analysis on a flashing LEDSAT has been presented as innovative study for the attitude determination. Moreover, the improvements associated to data fusion analysis of SLR measurements and optical data of a self-illuminated system have been underlined.

References

Abercromby, K.J., Seitzer, P., Cowardin, H.M., Barker, E.S., Matney, M. J., 2011. Michigan orbital debris survey telescope observations of the geosynchronous orbital debris environment observing years: 2007–2009, NASA/TP-2011-217350, Houston, TX, 2011.

Anz-Meador, P.D., 2017. CubeSat PMD by drag enhancement: mission planning for compliance with NASA standards. Orbit. Debris Quart. News 21 (2), 3–6.

Appleby, G.M., Bianco, G., Noll, C.E., Pavlis, E.C., Pearlman, M.R., 2016. Current trends and challenges in satellite laser ranging. In: IVS 2016 General Meeting Proceedings, Johannesburg, South Africa, 13-17 March, 2016, pp. 15–24.

Arena, L., Angeletti, F., Curianó, F., et al., 2015. Thermal and mechanical design and test campaign results of a single-piece structure for the URSA MAIOR nanosatellite. In: 66th International Astronautical Congress (IAC), Jerusalem, Israel, 12–16 October, 2015, vol. 7, pp. 6157–6163.

Arena, L., Piergentili, F., Santoni, F. et al., 2016. Integration and ground test campaign results of URSA MAIOR. In: 67th International Astronautical Congress (IAC), Guadalajara, Mexico, 26–30 September, 2016, vol. 6, pp. 3951–3958.

Brunet, M., Auriol, A., Agnieray, P., Nouel, F., 1995. DORIS precise orbit determination and localization system description and USOs performances. In: Proceedings of the 1995 IEEE International Frequency Control Symposium (49th Annual Symposium), San Francisco, California, USA, 31 May–2 June, 1995, pp. 122–132.

Cardona, T., Seitzer, P., Piergentili, F., Santoni, F., et al., 2017. Automatic pipeline for light-curves variability analysis of GEO objects. In: 7th European Conference on Space Debris, ESA Space Debris Office, Darmstadt, Germany, 18–21 April, 2017, published by the ESA Space Debris Office, Ed. Flohrer, T., Schmitz, F., vol. 7, Issue 1. Available at: <https://conference.sdo.esoc.esa.int/proceedings/sdc7/paper/301/SDC7-paper301.pdf>.

Cardona, T., Seitzer, P., Rossi, A., Piergentili, F., Santoni, F., 2016a. BVRI photometric observations and light-curve analysis of GEO objects. Adv. Space Res. 58 (4), 514–527. https://doi.org/10.1016/j.asr.2016.05.025.

Cardona, T., Seitzer, P., Rossi, A., et al., 2016. Analysis of the brightness variability of GEO objects. In: 67th International Astronautical Congress (IAC), Guadalajara, Mexico, 26–30 September, 2016, vol. 3, pp. 1631–1637.

Catalàn, M., Quijano, M., Pazos, A., et al., 2015. Space debris tracking at San Fernando laser station. In: 4th Workshop On Robotic Autonomous Observatories, Torremolinos, Spain, 28 September–2 October, 2015, pp. 103–106. Available at: <http://www.astroscu.unam.mx/rmaa/RMxAC.48/PDF/RMxAC.48_part-7.1.pdf>.

Chang, G., Xu, T., Wang, Q., 2016. Baseline configuration for GNSS attitude determination with an analytical least-squares solution. Meas. Sci. Technol. 27 (12). https://doi.org/10.1088/0957-0233/27/12/125105, Paper Number 125105.

Cordelli, E., Vananti, A., Schildknecht, T., 2016. Analysis of the orbit determination accuracy using laser ranges and angular measurements. In: 67th International Astronautical Congress (IAC), Guadalajara, Mexico, 26–30 September, 2016, vol. 4, pp. 2281–2289.

Hennegrave, L., Pyanet, M., Haag, H., Blanchet, G., Esmiller, B., Vial, S., Samain E., Paris, J., Albanese, D., 2013. Laser ranging with the MEO telescope to improve orbital accuracy of space debris. In: Proc. SPIE 8739, Sensors and Systems for Space Applications VI, 87390J, 21 May, 2013. https://doi.org/10.1117/12.2015365.

Howell, S., 2006. Handbook of CCD Astronomy, second ed. Cambridge University Press, Cambridge, pp. 50–52.

Howell, S., 2006. Handbook of CCD Astronomy, second ed. Cambridge University Press, Cambridge, pp. 66–67.

Howell, S., 2006. Handbook of CCD Astronomy, second ed. Cambridge University Press, Cambridge, pp. 73–74.

Howell, S., 2006. Handbook of CCD Astronomy, second ed. Cambridge University Press, Cambridge, pp. 116–121.

Kirchner, G., Grunwaldt, L., Neubert, R., et al., 2013. Laser ranging to nano-satellites in LEO orbits: plans, issues, simulations. In: 18th International Workshop on Laser Ranging, Fujiyoshida, Japan, 11–15 November, 2013, Proceeding paper 13-0222. Available at: <https://cddis.nasa.gov/lw18/docs/papers/Session6/13-02-22-Kirchner.pdf>.

Kirchner, G., Steindorfer, M., Wang, P., et al., 2017. Determination of attitude and attitude motion of space debris, using laser ranging and single-photon light-curve data. In: 7th European Conference on Space Debris, ESA Space Debris Office, Darmstadt, Germany, April, 18–21, 2017, published by the ESA Space Debris Office, Ed. Flohrer, T., Schmitz, F., vol. 7, Issue 1. Available at: <https://conference.sdo.esoc.esa.int/proceedings/sdc7/paper/696/SDC7-paper696.pdf>.

Kucharski, D., Kirchner, G., Koidl, F., et al., 2014. Attitude and spin period of space debris envisat measured by satellite laser ranging. IEEE Trans. Geosci. Remote Sens. 52, 7651–7657.

Liou, J.C., Johnson, N.L., 2016. Risks in space from orbiting debris. Science 311 (5759), 340–341. https://doi.org/10.1126/science.1121337.

Masillo, S., Morfei, D., Locatelli, G., Marmo, N., et al., 2017. A LED-based technology to improve the orbit determination of LEO satellite. In: 68th International Astronautical Congress (IAC), Adelaide, Australia, 25–29 September, 2017, vol. 6, pp. 4005–4013.

Nadarajah, N., Teunissen, P.J.G., Buist, P.J., 2012. Attitude determination of LEO satellites using an array of GNSS sensors. In: 15th International Conference on Information Fusion, Singapore, 9–12 July, 2012, pp. 1066–1072.

Nitschelm, C., 1988. Theoretical transmittance in the near UV, visible and near IR through the earth atmosphere for several observatories. Astron. Astrophys. Suppl. Ser. 74 (1), 67–72.

Piergentili, F., Santoni, F., Seitzer, P., et al., 2017. Attitude determination of orbiting objects from light-curve measurements. IEEE Trans. Aerosp. Electron. Syst. 53 (1), 81–90.

Pritchard, B.E., Rax, B.G., McClure, S., 2003. Recent radiation test results at JPL. In: IEEE Radiation Effects Data Workshop, Monterey, CA, USA, 25 July, 2003, pp. 24–337. Available at: <https://trs.jpl.nasa.gov/bitstream/handle/2014/38472/03-1928.pdf>.

Rousseau, G., Bostel, J., Mazari, B., 2005. Star recognition algorithm for APS star tracker: oriented triangles. IEEE Aerosp. Electron. Syst. Mag. 20, 27–31.

Schildknecht, T., Musci, R., Ploner, M., Flury, W., Kuusela, J., de Leon Cruz, J., de Fatima Dominguez Palmero, L., 2003. An optical search for small-size debris in GEO and GTO. In: Presented at 5th U.S.-Russian Space Surveillance Workshop, Pulkovo, St. Petersburg, Russia, 24–27 September, 2003. Available at: <http://aero.tamu.edu/sites/default/files/faculty/alfriend/Russia6thWorkshop/r5%20S5.2%20Schildknecht.pdf>.

Seitzer, P., Cutler, J., Piergentili, F., Santoni, F., et al., 2016. LEDsats: LEO CubeSats with LEDs for optical tracking. In: AMOS Technologies Conference, Wailea, Maui, Hawai'i, USA, 20–23 September, 2016, Ed. Ryan, S., The Maui Economic Development Board, id.115, pp. 1376–1379. Available at: <http://amostech.com/TechnicalPapers/2016/Poster/Seitzer.pdf>.

Seitzer, P., Piergentili, F., Santoni, F. et al., 2017. LEDSat: Design of a CubeSat equipped with LEDs as calibration target. In: 7th European Conference on Space Debris, ESA Space Debris Office, Darmstadt, Germany, 18–21 April, 2017, published by the ESA Space Debris Office, Ed. Flohrer, T., Schmitz, F., vol. 7, Issue 1. Available at: <https://conference.sdo.esoc.esa.int/proceedings/sdc7/paper/376/SDC7-paper376.pdf>.

Steindorfer, M.A., Kirchner, G., Koidl, F., Wang, P., Kucharski, D., 2017. Space debris science at the satellite laser ranging station Graz. In: 2017 IEEE International Conference on Environment and Electrical Engineering and 2017 IEEE Industrial and Commercial Power Systems Europe, Milan, Italy, 6–9 June, 2017, pp. 1278–1282. https://doi.org/10.1109/EEEIC.2017.7977641.

Somers, P., 2011. Cylindrical RSO signatures, spin axis orientation and rotation period determination, Advanced Maui Optical and Space Surveillance Technologies Conference, Wailea, Maui, Hawai'i, USA, 13–16 September, 2011, pp. 73–82, 2011, Edited by Ryan, S., The Maui Economic Development Board, 2011., id. E10. Available at: <https://amostech.com/TechnicalPapers/2011/NROC/SOMERS.pdf>.

Tanaka, T., Kawamura, Y., Tanaka, T., 2015. Development and operations of nano-satellite FITSAT-1 (NIWAKA). Acta Astronaut. 107 (February-March), 112–129. https://doi.org/10.1016/j.actaastro.2014.10.023.

Walsh, D.W., 2013. A survey of radars capable of providing small debris measurements for orbit prediction. Independent Paper, 2013. Available at: <https://pdfs.semanticscholar.org/presentation/ae05/5f65f723b498ddca561076728f7367434f1b.pdf>.

Websites

Inter-Agency Space Debris Coordination Committee, http://www.iadc-online.org/, visit: May 29th 2017.